



Article

---

# The Influence of Fly Ash and Slag on the Mechanical Properties of Geopolymer Concrete

---

Zhenyang Zhang, Tian Su, Lu Zhang, Run Zheng, Keshun Ma, Lin Zhang, Chiemela Victor Amaechi and Chunguang Wang

## Special Issue

Research on Properties and Usage of Construction Composite Materials

Edited by

Prof. Dr. Chunguang Wang and Dr. Tian Su



## Article

# The Influence of Fly Ash and Slag on the Mechanical Properties of Geopolymer Concrete

Zhenyang Zhang<sup>1</sup>, Tian Su<sup>1,2</sup> , Lu Zhang<sup>1</sup>, Run Zheng<sup>1</sup>, Keshun Ma<sup>1</sup>, Lin Zhang<sup>1</sup>, Chiemela Victor Amaechi<sup>3,4,5</sup>  and Chunguang Wang<sup>1,\*</sup> 

<sup>1</sup> School of Civil Engineering and Geomatics, Shandong University of Technology, Zibo 255000, China; zhangzhenyang0123@gmail.com (Z.Z.); sutian@sdut.edu.cn (T.S.); zlu@sdut.edu.cn (L.Z.); 22507020007@stumail.sdut.edu.cn (R.Z.); 23507030888@stumail.sdut.edu.cn (K.M.); 23507030875@stumail.sdut.edu.cn (L.Z.)

<sup>2</sup> Department of Engineering and Management, International College, Krirk University, No. 3 Soi Ramintra 1, Ramintra Road, Anusaowaree, Bangkok 10220, Thailand

<sup>3</sup> School of Engineering, Lancaster University, Lancaster LA1 4YW, UK; chiemelavic@gmail.com

<sup>4</sup> Department of Construction Management, Global Banking School, Devonshire Street North, Manchester M12 6JH, UK

<sup>5</sup> Institute of Energy Infrastructure, National Energy University, Kajang 43009, Malaysia

\* Correspondence: cgwang@sdut.edu.cn

**Abstract:** The use of geopolymer as a cementitious material for geopolymer concrete (GPC) is beneficial for the sustainable development and green transformation of the construction industry. Geopolymer concrete has many advantages, such as high strength, heat and corrosion resistance, low hydration heat, and carbon emissions. This paper adopted the water–binder ratio, alkaline activator modulus, and slag replacement as the influencing factors, and used the 28-day compressive strength and flexural strength of geopolymer concrete as the response values to seek a reasonable mix design. In addition, through microstructure analysis, the mechanism of geopolymer on concrete was studied. The results indicated that as the water–binder ratio increased, the compressive strength first increased and then decreased, while the flexural strength continuously decreased. As the amount of slag replacement increased, the compressive strength and flexural strength would also increase. The effect of alkaline activator modulus on compressive strength and flexural strength was not significant. Through response surface methodology (RSM) analysis, the optimal design of geopolymer concrete was determined to have a water–cement ratio of 3.50, a modulus of 1.54 for alkaline activator solution, and a slag substitution rate of 47%. The microstructure analysis showed that the water–binder ratio and slag replacement improved the pore structure and density of concrete, thereby enhancing the macroscopic mechanical properties of concrete. This paper can provide a theoretical basis for the application of geopolymer concrete in engineering.

**Keywords:** geopolymer concrete; fly ash; slag; response surface methodology; compressive strength; flexural strength; microstructure



**Citation:** Zhang, Z.; Su, T.; Zhang, L.; Zheng, R.; Ma, K.; Zhang, L.; Amaechi, C.V.; Wang, C. The Influence of Fly Ash and Slag on the Mechanical Properties of Geopolymer Concrete. *Buildings* **2024**, *14*, 2720. <https://doi.org/10.3390/buildings14092720>

Academic Editor: Bjorn Birgisson

Received: 30 July 2024

Revised: 23 August 2024

Accepted: 28 August 2024

Published: 30 August 2024



**Copyright:** © 2024 by the authors. Licensee MDPI, Basel, Switzerland. This article is an open access article distributed under the terms and conditions of the Creative Commons Attribution (CC BY) license (<https://creativecommons.org/licenses/by/4.0/>).

## 1. Introduction

Concrete is extensively utilized in engineering fields such as roads, bridges, and buildings [1–4], and stands as one of the widely used construction materials globally [5–7]. The fundamental components of concrete are cementitious materials, coarse and fine aggregates, and water, some of which may be supplemented with other additives and admixtures [8,9]. Ordinary silicate cement is the most commonly used cementitious material in concrete preparation [10,11], and the global production of ordinary Portland cement (OPC) is reported to exceed 4.4 billion tons per year [12,13]. However, the production of OPC entails significant energy consumption and environmental pollution; for instance,

1 ton of OPC requires the consumption of 3200–5500 MJ of thermal energy [14,15], while releasing about 0.8–1 tons of harmful gases [16], thereby exacerbating the greenhouse effect [17,18]. The cement industry contributes approximately 8% to the world's total carbon emissions in terms of CO<sub>2</sub> [16,19,20]. In order to harmonize building development with green low-carbon initiatives [21,22], it is essential to replace OPC with environmentally friendly cementitious materials [23].

The concept of geopolymers was initially introduced by Joseph Davidovits [24] in the 1970s. According to the different activators, geopolymers could be divided into alkali-activated geopolymers, acid-activated geopolymers, and salt-activated geopolymers [25–27]. Generally speaking, alkaline activators have good excitation effects and result in high strength. Alkali-activated geopolymer is an inorganic cementitious material formed through a series of reactions involving substances rich in silicon and aluminum, catalyzed by alkaline activators [28,29]. During the reaction process, the T (Si, Al)–O chemical bonds in the aluminosilicate material break (depolymerize) under the influence of hydroxyl (OH<sup>-</sup>) groups, subsequently leading to condensation reactions which form a three-dimensional network structure composed of silicon and aluminum oxygen tetrahedra, connected by shared oxygen atoms [30,31]. The dissolution mechanism determines whether the active ingredients of the material can be fully released, which directly affects the subsequent nucleation process. The nucleation mechanism determines the structure and properties of geopolymers, while the nucleation process determines the strength and durability of GPC. Raw materials for geopolymers come from a wide range of sources, such as metakaolin [32], silica fume [33], clays [34], lithium slag [35], red mud [36], rice husk [37], gangue [38], fly ash [39], slag [40]. Metakaolin has high pozzolanic activity which contributes to the formation of a more uniform and denser network for the structure, thereby improving the elastic modulus of the concrete. Meanwhile, it can quickly release silicate and aluminate ions in an alkaline environment, leading to a higher early strength and faster hardening rate. Comparatively speaking, the activity of fly ash is generally not as strong as metakaolin, that is to say, the reaction rate is slower, and the setting time would be extended. Hence, slag with high calcium content is normally used together to improve the reaction rate and reduce the setting time. Compared to metakaolin, the environmental friendliness of fly ash and slag is more significant. The biggest advantage of geopolymers is their low-temperature requirement for synthesis reaction, simple preparation process, and low energy consumption for production [41]. Geopolymer production consumes about 40% less energy than OPC's consumption [42] and the carbon emissions from geopolymer preparation are only 10–20% of those from OPC's preparation [43]. Therefore, using geopolymer as a cementitious material for geopolymer concrete (GPC) is conducive to sustainable development and green transformation of the construction industry.

GPC exhibits excellent performance with high strength [44–47], heat and corrosion resistance [48–53], low heat of hydration [54,55], and low carbon emissions [56,57]. However, the achievement of these properties requires a rational mix ratio design. From a study using a one-factor test method [58], it was found that both 28-day compressive strength and fluidity increased with an increase in Na<sub>2</sub>SiO<sub>3</sub> to NaOH ratio, while the increase in water to cement ratio led to the increase in fluidity and reduction in strength. In order to comprehensively assess the effects of various factors, an orthogonal test method was then utilized to optimize the mix ratios of GPC and concluded that the water–cement ratio is the most important factor affecting the properties of GPC [59]. Ponalagappan et al. used the Taguchi method [60] to design the mix ratios, and the analysis of variance showed that the ratio of excitors to precursors and the slag admixture were the most significant factors affecting the compressive strength. Li N [61] used the simplex barycenter design method to study the mix ratio of GPC in slag base, and the results showed that the water–binder ratio and the ratio of Na<sub>2</sub>O to the cementable material were the key factors affecting the compressive strength and setting time. However, the simplex barycentric design method did not perform well in non-convex optimization problems.

Compared to the mentioned design methods in last paragraph, response surface methodology (RSM) can reduce the number of tests and obtain a continuous model [62], and has been applied to the optimization of construction material ratios in recent years [63,64]. More specifically, RSM is an optimization method that integrates experimental design and mathematical modeling [65,66], in which certain experimental data are obtained through scientific experimental design and regression equations are used to fit the functional relationship between the influencing factors and the response values [67–69].

In this paper, the RSM was used to design and optimize the proportion of GPC. The water–binder ratio, modulus of alkali exciter solution, and slag replacement were selected as the influencing factors, while the 28-day compressive strength and flexural strength of the GPC were set as the response values. A regression equation was used to fit the functional relationship between the influencing factors and the response values. Then, a response surface model for the compressive strength and flexural strength of GPC was proposed to quantify the effects of various influencing factors on the compressive and flexural strengths of GPC. Also, a scanning electron microscopy (SEM) test was conducted to analyze the mechanism of the mechanical properties of GPC, according to the effect of different design factors. Based on the proposed model, it is possible to quickly obtain a mix proportion of GPC that simultaneously achieves the optimal compressive and flexural strengths without conducting multiple repeated tests. This would provide better convenience and acceptability for the application of GPC in engineering practice.

## 2. Materials and Methods

### 2.1. Raw Materials

The binder material used in the study was fly ash and slag. Fly ash is a byproduct of the combustion of coal, normally in the form of spherical particles [70]. Slag, derived from blast furnace slag, is a byproduct of the ironmaking process [71]. The utilized fly ash was Class II, F, with a sieve residue of 19.9% in the 45  $\mu\text{m}$  sieve and a loss on burnout of 1.1%. Here, we have to note that fly ash of Class F has lower calcium content, leading to a higher degree of pozzolanic activities, regardless of its particle size [72]. The utilized slag was grade S95, with a density of 2.88  $\text{g}/\text{cm}^3$ , a specific surface area of 445  $\text{m}^2/\text{kg}$ , and a loss on burnout of 0.55%. The chemical composition of fly ash and slag is presented in Table 1. The morphology of fly ash and slag used in the test is illustrated in Figure 1.

**Table 1.** Chemical composition of fly ash and slag.

Chemical Composition	Mass Fraction/%	
	Fly Ash	Slag
SiO <sub>2</sub>	55.04	28.11
Al <sub>2</sub> O <sub>3</sub>	25.50	12.36
CaO	4.39	42.99
SO <sub>3</sub>	3.23	2.08
Fe <sub>2</sub> O <sub>3</sub>	3.76	1.82
K <sub>2</sub> O	1.87	1.26
Na <sub>2</sub> O	1.74	0.60
MgO	1.58	5.32
TiO <sub>2</sub>	1.16	1.93
SrO	0.87	0.14
MnO	0.12	2.75
P <sub>2</sub> O <sub>5</sub>	0.27	0.45
Cl	0.21	0.18



**Figure 1.** Morphology of fly ash and slag used in the test. (a) Fly ash; (b) Slag.

The concentration, particle size, and chemical properties of different activators can affect the formation rate and final structure of GPC, and research showed that using a mixed activator offered more advantages than using a single one [73]. The alkaline exciter solution in the study was a mixture of sodium silicate and sodium hydroxide. More specifically, water was the common tap water, and sodium hydroxide was commercially available with analytically pure  $\geq 96\%$ . The specific indicators of sodium silicate solution are shown in Table 2. Figure 2 illustrates the schematic diagram of the preparation method for alkali exciter solution.

**Table 2.** Indicators of sodium silicate solution.

Concentration/(°Bé)	Sodium Silicate Modulus	Mass Fraction/%		
		H <sub>2</sub> O	Na <sub>2</sub> O	SiO <sub>2</sub>
40	3.29	65.85	8.15	26

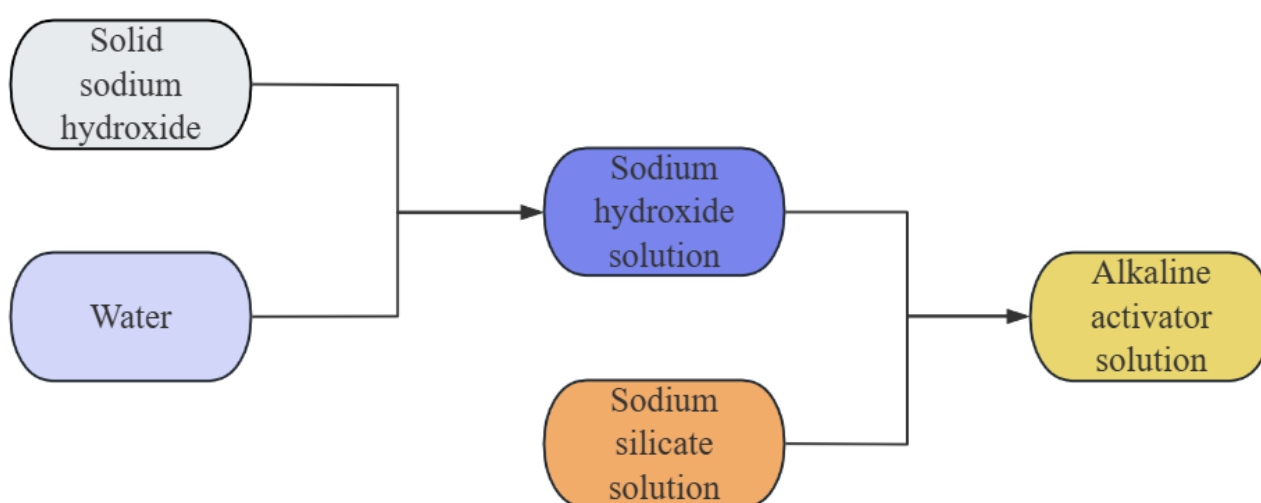


**Figure 2.** Schematic diagram of preparation method for alkaline activator solution.

The fine aggregate was natural river sand, and the coarse aggregate was crushed stone. The physical properties of the aggregates are presented in Table 3. Sieve tests

were conducted using square sieves with various mesh sizes to assess the particle size distribution of aggregates, and the results are illustrated in Figure 3.

**Table 3.** Table of aggregate properties.

Material	Specific Gravity	Compacted Dry Density ( $\text{kg/m}^3$ )	Water Absorption (%)	Fineness Modulus
Natural sand	2.96	1710	1.30	2.96
Crushed stone	2.88	1675	0.58	6.65

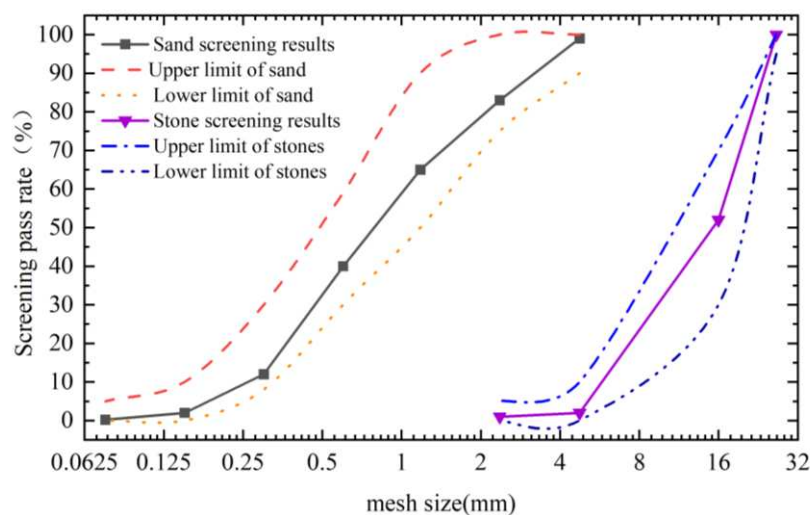


**Figure 3.** Aggregate particle grading table.

## 2.2. Response Surface Method

RSM encompasses a comprehensive array of design methodologies, including full factorial design [74], central composite design [75], Box–Behnken design [61] and Doehlert matrix design [76], etc., which can be used to select the appropriate design method according to the actual conditions. In this study, the Box–Behnken design was selected due to the integration of efficiency, cost, and required accuracy.

The water–binder ratio, alkali activator modulus, and slag replacement, which are closely linked to the performance of geopolymer concrete, are represented by A, B, and C, respectively. Although a lower water–binder ratio could lead to higher strength of GPC, it also might result in excessive shrinkage and the formation of cracks. The replacement of slag could enhance the activity of GPC, thereby eliminating the curing process at high temperatures and increasing the strength of the prepared GPC. However, due to the high calcium content in slag, the reaction speed would be too fast, and the setting time would be too short, if the replacement of slag was too high. This would be detrimental to the workability of GPC. Based on preliminary experiments and literature review [41,47,77–79], the water–binder ratio (0.34–0.42), alkali exciter solution modulus (1.0–1.6) and slag replacement (10–50%) were identified as the influencing factors (Table 4), while the compressive strength and flexural strength of GPC were served as the response values. Take the determination of the water–binder ratio as an example: a wider range of water–binder ratios was obtained from related literature firstly, and then the preliminary experiment was conducted to examine the workability with different water–binder ratios, thereby narrowing and determining the range of water–binder ratio as 0.34–0.42.

A response surface model was fitted according to the experimental results and this model analyzed the influence of each factor on the response value. In the end, the integrated maximum values of compressive strength and flexural strength and the corresponding optimal parameter level can be identified.

**Table 4.** Coding level table.

Influence Factor	Code	Level		
		−1	0	1
Water–binder ratio	A	0.34	0.38	0.42
Alkaline activator modulus	B	1	1.3	1.6
Slag replacement	C	10%	30%	50%

Response surface modelling reflects the functional relationship between the influencing factors and the response values. In order to determine whether there was a statistically significant relationship between them, an analysis of variance (ANOVA) was also conducted. The overall significance of the linear equation was evaluated by examining the mean situation of the data through the F-test. The  $p$ -value was a decreasing indicator of the degree of confidence in the results and the level of significance was taken as 0.05. When the  $p$ -value  $\leq 0.05$ , it indicated that the result was statistically significant. The F-value was calculated using the Equations (1)–(3):

$$SSR = \sum_{i=1}^n (\hat{y}_i - \bar{y}) \quad (1)$$

$$SSE = \sum_{i=1}^n (y_i - \hat{y}_i) \quad (2)$$

$$F = \frac{SSR/p}{SSE/n - p - 1} \quad (3)$$

Here,

$y_i$  is the experimental value;  $\hat{y}_i$  is the predicted value of the model;  $\bar{y}$  is the average of the experimental values;  $SSR$  is the sum of regression squares;  $SSE$  is the sum of squared errors;  $p$  is the degree of freedom of  $SSR$ ;  $n - p - 1$  is the degree of freedom of  $SSE$ .

The coefficient of determination  $R^2$  was used to evaluate the goodness of fit of the model, with a value between 0 and 1. The closer  $R^2$  was to 1, the better the model was fitted.  $R^2$  was calculated using Equations (4) and (5):

$$SST = SSR + SSE \quad (4)$$

$$R^2 = 1 - \frac{SSE}{SST} \quad (5)$$

Here,

$SST$  is the sum of squared total deviations;  $R^2$  is the model determination coefficient.

In addition, the adjustment coefficient of determination ( $R_a^2$ ) was used to increase the model's simplicity while ensuring the model's reliability by eliminating the terms that do not improve the model's accuracy (Equation (6)). It was analyzed together with the prediction coefficient of determination ( $R_p^2$ ), which reflected the predictive ability of the model (Equation (7)). It required that the difference between  $R_a^2$  and  $R_p^2$  did not exceed 0.2. Also, the coefficient of variation (C.V.) was required to be less than 10% (Equation (8)).

$$R_a^2 = 1 - \frac{(1 - R^2)(n - 1)}{n - p - 1} \quad (6)$$

$$R_p^2 = 1 - \frac{\sum_{i=1}^n (y_i - \hat{y}_i)^2}{SST} \quad (7)$$

$$\text{C.V.} = \frac{\sigma}{\mu} \quad (8)$$

Here,

$R_a^2$  is adjustment coefficient of determination;  $R_p^2$  is the prediction coefficient of determination; C.V. is the coefficient of variation;  $\sigma$  is the standard deviation;  $\mu$  is the mean value.

### 2.3. Mixing Ratio Design and Preparation

The GPC in the study was designed with a water–binder ratio, modulus of alkali exciter solution, and slag replacement to study their effects on the compressive and flexural strengths.

Based on preliminary tests and relevant literature [41,47,77–79], the range of influencing factors was identified. The water–binder ratios were taken as 0.34, 0.38 and 0.42, the alkaline activator moduli were taken as 1.0, 1.3 and 1.6, and the slag replacements were taken as 10%, 30% and 50%, as showed in Table 4. The density of the GPC was set at 2400 kg/m<sup>3</sup>, the sodium silicate solution at 147.04 kg/m<sup>3</sup>, and the sand rate at 0.4.

The experimental design was based on three factors, three levels and five centroids, resulting in a total of 17 groups. Here, 12 groups were analytical factor tests, while the remaining 5 groups were replicated tests at the centroids of the designed area, with the objective of determining the experimental errors. The mix ratios of each group are presented in Table 5.

**Table 5.** Mix design proportions for GPC.

No.	Water–Binder Ratio	Alkaline Activator Modulus	Slag Replacement	Mix Proportion/(kg/m <sup>3</sup> )							
				Fly Ash	Slag	Sodium Silicate	Sodium Hydroxide	Water	Fine Aggregate	Coarse Aggregate	
I	1	0.38	1.3	30%	297.34	127.43	147.04	23.68	93.18	694	1041
	2	0.38	1.3	30%	297.34	127.43	147.04	23.68	93.18	694	1041
	3	0.38	1.3	30%	297.34	127.43	147.04	23.68	93.18	694	1041
II	1	0.34	1.3	50%	212.39	212.39	147.04	23.68	73.18	702	1053
	2	0.34	1.3	50%	212.39	212.39	147.04	23.68	73.18	702	1053
	3	0.34	1.3	50%	212.39	212.39	147.04	23.68	73.18	702	1053
III	1	0.38	1.3	30%	297.34	127.43	147.04	23.68	93.18	694	1041
	2	0.38	1.3	30%	297.34	127.43	147.04	23.68	93.18	694	1041
	3	0.38	1.3	30%	297.34	127.43	147.04	23.68	93.18	694	1041
IV	1	0.38	1.6	50%	212.39	212.39	147.04	16.34	93.18	694	1041
	2	0.38	1.6	50%	212.39	212.39	147.04	16.34	93.18	694	1041
	3	0.38	1.6	50%	212.39	212.39	147.04	16.34	93.18	694	1041
V	1	0.34	1.0	30%	297.34	127.43	147.04	35.42	73.18	702	1053
	2	0.34	1.0	30%	297.34	127.43	147.04	35.42	73.18	702	1053
	3	0.34	1.0	30%	297.34	127.43	147.04	35.42	73.18	702	1053
VI	1	0.34	1.6	30%	297.34	127.43	147.04	16.34	73.18	702	1053
	2	0.34	1.6	30%	297.34	127.43	147.04	16.34	73.18	702	1053
	3	0.34	1.6	30%	297.34	127.43	147.04	16.34	73.18	702	1053
VII	1	0.38	1.0	50%	212.39	212.39	147.04	35.42	93.18	694	1041
	2	0.38	1.0	50%	212.39	212.39	147.04	35.42	93.18	694	1041
	3	0.38	1.0	50%	212.39	212.39	147.04	35.42	93.18	694	1041
VIII	1	0.42	1.3	50%	212.39	212.39	147.04	23.68	113.18	686	1029
	2	0.42	1.3	50%	212.39	212.39	147.04	23.68	113.18	686	1029
	3	0.42	1.3	50%	212.39	212.39	147.04	23.68	113.18	686	1029
IX	1	0.42	1.0	30%	297.34	127.43	147.04	35.42	113.18	686	1029
	2	0.42	1.0	30%	297.34	127.43	147.04	35.42	113.18	686	1029
	3	0.42	1.0	30%	297.34	127.43	147.04	35.42	113.18	686	1029
X	1	0.38	1.0	10%	382.30	42.48	147.04	35.42	93.18	694	1041
	2	0.38	1.0	10%	382.30	42.48	147.04	35.42	93.18	694	1041
	3	0.38	1.0	10%	382.30	42.48	147.04	35.42	93.18	694	1041
XI	1	0.38	1.6	10%	382.30	42.48	147.04	16.34	93.18	694	1041
	2	0.38	1.6	10%	382.30	42.48	147.04	16.34	93.18	694	1041
	3	0.38	1.6	10%	382.30	42.48	147.04	16.34	93.18	694	1041
XII	1	0.38	1.3	30%	297.34	127.43	147.04	23.68	93.18	694	1041
	2	0.38	1.3	30%	297.34	127.43	147.04	23.68	93.18	694	1041
	3	0.38	1.3	30%	297.34	127.43	147.04	23.68	93.18	694	1041
XIII	1	0.38	1.3	30%	297.34	127.43	147.04	23.68	93.18	694	1041
	2	0.38	1.3	30%	297.34	127.43	147.04	23.68	93.18	694	1041
	3	0.38	1.3	30%	297.34	127.43	147.04	23.68	93.18	694	1041
XIV	1	0.38	1.3	30%	297.34	127.43	147.04	23.68	93.18	694	1041
	2	0.38	1.3	30%	297.34	127.43	147.04	23.68	93.18	694	1041
	3	0.38	1.3	30%	297.34	127.43	147.04	23.68	93.18	694	1041

Table 5. Cont.

No.	Water–Binder Ratio	Alkaline Activator Modulus	Slag Replacement	Mix Proportion/(kg/m <sup>3</sup> )							
				Fly Ash	Slag	Sodium Silicate	Sodium Hydroxide	Water	Fine Aggregate	Coarse Aggregate	
XV	1	0.42	1.3	10%	382.30	42.48	147.04	23.68	113.18	686	1029
	2	0.42	1.3	10%	382.30	42.48	147.04	23.68	113.18	686	1029
	3	0.42	1.3	10%	382.30	42.48	147.04	23.68	113.18	686	1029
XVI	1	0.42	1.6	30%	297.34	127.43	147.04	16.34	113.18	686	1029
	2	0.42	1.6	30%	297.34	127.43	147.04	16.34	113.18	686	1029
	3	0.42	1.6	30%	297.34	127.43	147.04	16.34	113.18	686	1029
XVII	1	0.34	1.3	10%	382.30	42.48	147.04	23.68	73.18	702	1053
	2	0.34	1.3	10%	382.30	42.48	147.04	23.68	73.18	702	1053
	3	0.34	1.3	10%	382.30	42.48	147.04	23.68	73.18	702	1053

The GPC was prepared in the following steps:

1. Fly ash and slag were mixed for 120 s;
2. Aggregates were added and mixed for a further 120 s;
3. Alkali stimulant solution was added and mixed for a further 180 s to obtain a homogeneous GPC mix;
4. GPC mix was poured into the mould and placed on the vibrating table for 60 s to remove air bubbles and improve the compactness;
5. The mould was covered with a film to prevent water evaporation and the specimens were demoulded after 24 h at room temperature;
6. Specimens were subjected to a curing process at a temperature of  $20 \pm 2$  °C and a humidity of  $\geq 95\%$  for a period of 28 days, after which they were tested for mechanical properties.

#### 2.4. Test Methods

##### 2.4.1. Mechanical Properties Test Methods

The mechanical tests of GPC were conducted referring to GB/T 50081-2019 [80] and GB/T 50107-2010 [81].

For the compressive strength test, a specimen with the size of 100 mm × 100 mm × 100 mm was utilized and tested at a loading rate of 0.5 MPa/s. The compressive strength was calculated using Equation (9).

$$f_c = 0.95 \times \frac{F}{A} \quad (9)$$

Here,

$f_c$  is the compressive strength of the specimen (MPa); 0.95 is the size conversion factor for non-standard specimens;  $F$  is the ultimate load of the specimen (N);  $A$  is the specimen cross-section area (mm<sup>2</sup>).

For the flexural strength test, a specimen with the size of 100 mm × 100 mm × 400 mm was selected and tested at a loading speed of 0.2 kN/s. The flexural strength was calculated using Equation (10).

$$f_f = 0.85 \times \frac{FL}{bh^2} \quad (10)$$

Here,

$f_f$  is the flexural strength of the specimen (MPa); 0.85 is the size conversion factor for non-standard specimens;  $F$  is the ultimate load of the specimen (N);  $L$  is the distance between supports;  $b$  is the width of the specimen;  $h$  is the height of the specimen.

##### 2.4.2. Microscopic Test Methods

The microscopic morphology of the crushed GPC specimens was obtained by microscopic tests using a scanning electron microscope (SEM) and the following steps were employed:

1. Clean the sample table with an alcohol cotton ball and blow dry;
2. Fix the specimen pieces to the sample stage using conductive adhesive;
3. Carry out the vacuuming and gold-spraying step;
4. Perform the test using SEM and pick up the images at the desired magnification.

### 3. Results and Discussion

Before conducting the compressive and flexural strength tests, the workability of GPC was tested, and the obtained results of slump and water retention for each group of GPC mixture satisfied the relevant regulatory requirements.

#### 3.1. Experimental Results

The 28 d compressive strength and 28 d flexural strength of each group of GPC are presented in Table 6.

**Table 6.** Experimental test results.

Test Group No.	Compressive Strength/MPa				Flexural Strength/MPa			
	1	2	3	Test Value	1	2	3	Test Value
I	63.1	68.3	64.6	65.4	3.45	3.38	3.20	3.35
II	69.4	83.1	81.8	81.8	4.54	3.77	3.53	3.77
III	69.0	66.0	73.4	69.5	3.62	3.48	3.51	3.54
IV	83.0	85.6	88.0	85.5	3.86	3.87	3.75	3.83
V	60.7	53.4	56.2	56.7	3.88	3.43	3.20	3.50
VI	62.3	64.9	60.8	62.5	3.43	3.17	3.02	3.20
VII	67.3	76.4	68.8	70.8	3.61	3.08	3.38	3.36
VIII	77.2	78.6	68.6	74.7	2.93	3.11	3.28	3.11
IX	57.6	54.5	51.3	54.4	2.66	2.84	2.45	2.65
X	46.1	43.8	41.7	43.8	2.42	2.42	2.46	2.44
XI	20.3	18.0	18.5	18.9	2.02	1.92	1.69	1.88
XII	60.7	62.1	61.0	61.3	3.17	3.01	3.20	3.13
XIII	59.8	63.6	73.6	63.6	3.50	3.28	3.29	3.36
XIV	69.9	67.4	60.9	66.0	3.39	3.21	3.26	3.29
XV	21.0	19.4	20.5	20.3	1.44	1.47	1.54	1.48
XVI	46.9	46.5	46.3	46.6	2.65	2.46	2.55	2.55
XVII	24.9	26.2	25.0	25.4	2.40	2.45	1.93	2.40

#### 3.2. Response Surface Fitting and Validation

Based on the test results, the multivariate regression equations between water–binder ratio ( $A$ ), modulus of alkali exciter solution ( $B$ ), slag admixture ( $C$ ) and 28 d compressive strength ( $Y_1$ ), 28 d flexural strength ( $Y_2$ ) were established (Equations (11) and (12)).

Compressive strength:

$$Y_1 = 65.16 - 3.80 \times A - 1.52 \times B + 25.55 \times C - 3.40 \times AB - 0.50 \times AC + 9.90 \times BC - 7.16 \times A^2 - 2.96 \times B^2 - 7.45 \times C^2 \quad (11)$$

Flexural strength:

$$Y_2 = 3.33 - 0.39 \times A - 0.061 \times B + 0.73 \times C + 0.050 \times AB + 0.065 \times AC + 0.26 \times BC - 0.27 \times A^2 - 0.086 \times B^2 - 0.37 \times C^2 \quad (12)$$

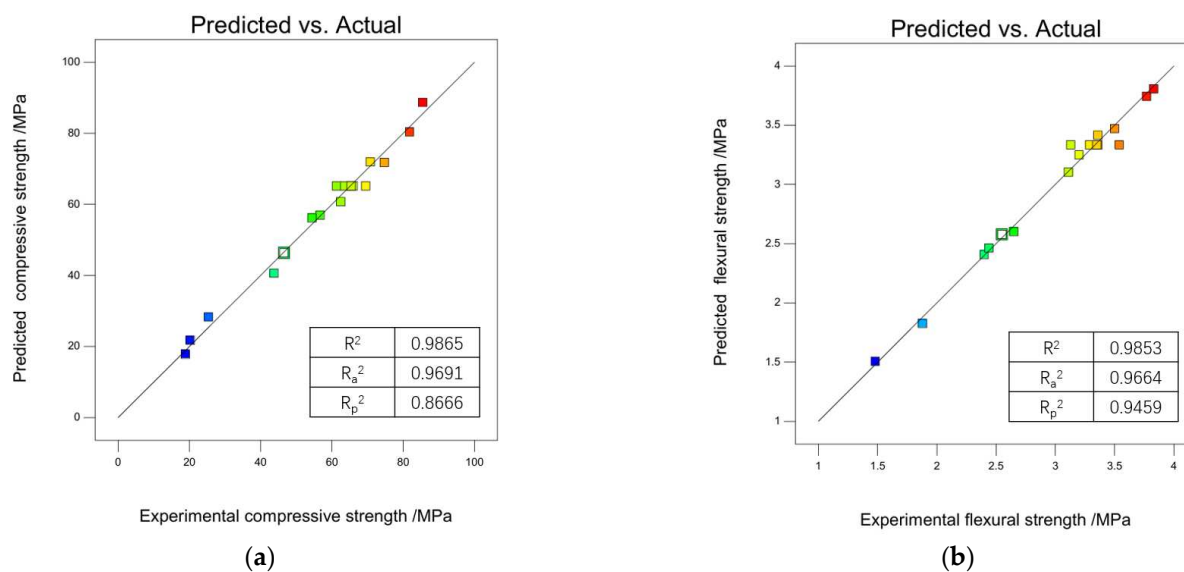
The predicted and tested results, along with the corresponding relative errors, are presented in Table 7. Meanwhile, Figure 4 depicts a comparison chart between the predicted and tested values, and as illustrated in Figure 4, the discrepancy was minimal, indicating a high degree of accuracy in the model's prediction.

Table 7. Actual strength and predicted strength.

No.	Compressive Strength			Flexural Strength			
	Measured Value/MPa	Predicted Value/MPa	Relative Error/%	Measured Value/MPa	Predicted Value/MPa	Relative Error/%	
I	1	63.1	3.3	3.45		−3.48	
	2	68.3		3.38		−1.48	
	3	64.6	65.2	0.9	3.20	3.33	4.06
	Test value	65.4		−0.3	3.35		−0.60
II	1	69.4		15.9	4.54	−17.62	
	2	83.1	80.4	−3.2	3.77	−0.80	
	3	81.8		−1.7	3.53	3.74	5.95
	Test value	81.8		−1.7	3.77		−0.80
III	1	69.0		−5.5	3.62	−8.01	
	2	66.0	65.2	−1.2	3.48	3.33	−4.31
	3	73.4		−11.2	3.51		−5.13
	Test value	69.5		−6.2	3.54		−5.93
IV	1	83.0		6.9	3.86	−1.30	
	2	85.6	88.7	3.6	3.87	3.81	−1.55
	3	88.0		0.8	3.75		1.60
	Test value	85.5		3.7	3.83		−0.52
V	1	60.7		−6.1	3.88	−10.57	
	2	53.4	57.0	6.7	3.43	3.47	1.17
	3	56.2		1.4	3.20		8.44
	Test value	56.7		0.5	3.50		−0.86
VI	1	62.3		−2.6	3.43	−5.25	
	2	64.9	60.7	−6.5	3.17	3.25	2.52
	3	60.8		−0.2	3.02		7.62
	Test value	62.5		−2.9	3.20		1.56
VII	1	67.3		6.8	3.61	−5.26	
	2	76.4	71.9	−5.9	3.08	3.42	11.04
	3	68.8		4.5	3.38		1.18
	Test value	70.8		1.6	3.36		1.79
VIII	1	77.2		−7.0	2.93	5.80	
	2	78.6	71.8	−8.7	3.11	3.10	−0.32
	3	68.6		4.7	3.28		−5.49
	Test value	74.7		−3.9	3.11		−0.32
IX	1	57.6		−2.4	2.66	−2.26	
	2	54.5	56.2	3.1	2.84	2.60	−8.45
	3	51.3		9.6	2.45		6.12
	Test value	54.4		3.3	2.65		−1.89
X	1	46.1		−11.9	2.42	1.65	
	2	43.8	40.6	−7.3	2.42	2.46	1.65
	3	41.7		−2.6	2.46		0.00
	Test value	43.8		−7.3	2.44		0.82
XI	1	20.3		−12.3	2.02	−9.41	
	2	18.0	17.8	−1.1	1.92	1.83	−4.69
	3	18.5		−3.8	1.69		8.28
	Test value	18.9		−5.8	1.88		−2.66
XII	1	60.7		7.4	3.17	5.05	
	2	62.1	65.2	5.0	3.01	3.33	10.63
	3	61.0		6.9	3.20		4.06
	Test value	61.3		6.4	3.13		6.39
XIII	1	59.8		9.0	3.50	−4.86	
	2	63.6	65.2	2.5	3.28	3.33	1.52
	3	73.6		−11.4	3.29		1.22
	Test value	63.6		2.5	3.36		−0.89

Table 7. Cont.

No.	Compressive Strength			Flexural Strength			
	Measured Value/MPa	Predicted Value/MPa	Relative Error/%	Measured Value/MPa	Predicted Value/MPa	Relative Error/%	
XIV	1	69.9	−6.7	3.39		−1.77	
	2	67.4	−3.3	3.21		3.74	
	3	60.9	65.2	7.1	3.26	3.33	2.15
	Test value	66.0		−1.2	3.29		1.22
XV	1	21.0	3.3	1.44		4.86	
	2	19.4	21.7	11.9	1.47	1.51	2.72
	3	20.5		5.9	1.54		−1.95
	Test value	20.3		6.9	1.48		2.03
XVI	1	46.9	−1.3	2.65		−2.64	
	2	46.5	−0.4	2.46		4.88	
	3	46.3	46.3	0.0	2.55	2.58	1.18
	Test value	46.6		−0.6	2.55		1.18
XVII	1	24.9	13.7	2.40		0.42	
	2	26.2	28.3	8.0	2.45	2.41	−1.63
	3	25.0		13.2	1.93		24.87
	Test value	25.4		11.4	2.40		0.42



**Figure 4.** Comparison between predicted actual strength and predicted strength. (a) Compressive strength; (b) Flexural strength.

ANOVA was used to analyze the effect of variables on the response values and to determine the most significant factor. The level of significance in this study was 0.05, i.e., when the  $p$ -value is  $\leq 0.05$ , the model or factor is considered significant [82]. Table 8 shows the ANOVA results of the regression equation.

As illustrated in Table 8, the  $F$ -values and  $p$ -values of the models developed for 28 d compressive strength ( $Y_1$ ) and 28 d flexural strength ( $Y_2$ ) were 56.71,  $<0.0001$  and 52.07,  $<0.0001$ , respectively. On the other hand, the  $p$ -values of Lack of Fit were 0.2865 and 0.8721, respectively for  $Y_1$  and  $Y_2$ . This demonstrated that the regression models were highly significant with good statistical significance.

For  $Y_1$ , the  $p$ -values for the single factors  $A$ ,  $B$ , and  $C$  were 0.0185, 0.2603, and  $<0.0001$ , respectively, indicating that factors  $A$  and  $C$  had a significant effect on  $Y_1$ , while factor  $B$  had a non-significance. The  $p$ -values for the two-factor interaction  $AB$ ,  $AC$ , and  $BC$  were

0.0948, 0.7847, and 0.0008, respectively, indicating that factor *BC* had a significant effect on  $Y_1$ , while factors *AB* and *AC* had a non-significance.

**Table 8.** Analysis of variance.

Response	Source	Sum of Squares	Degree of Freedom	Mean Square	F-Value	<i>p</i> -Value	Notes	
$Y_1$	Model	6330.43	9	703.38	56.71	<0.0001	significant	
	<i>A</i>	115.52	1	115.52	9.31	0.0185		
	<i>B</i>	18.60	1	18.60	1.50	0.2603		
	<i>C</i>	5222.42	1	5222.42	421.08	<0.0001		
	<i>AB</i>	46.24	1	46.24	3.73	0.0948		
	<i>AC</i>	1.00	1	1.00	0.081	0.7847		
	<i>BC</i>	392.04	1	392.04	31.61	0.0008		
	$A^2$	215.55	1	215.55	17.38	0.0042		
	$B^2$	36.77	1	36.77	2.96	0.1288		
	$C^2$	234.01	1	234.01	18.87	0.0034		
	Residual	86.82	7	12.40				
	Lack of Fit	49.88	3	16.63	1.80	0.2865		not significant
	Pure Error	36.93	4	9.23				
	Cor Total	6417.25	16					
$Y_2$	Model	6.82	9	0.76	52.07	< 0.0001	significant	
	<i>A</i>	1.19	1	1.19	81.50	< 0.0001		
	<i>B</i>	0.030	1	0.030	2.06	0.1941		
	<i>C</i>	4.31	1	4.31	296.04	< 0.0001		
	<i>AB</i>	0.01	1	0.01	0.69	0.4344		
	<i>AC</i>	0.017	1	0.017	1.16	0.3169		
	<i>BC</i>	0.27	1	0.27	18.23	0.0037		
	$A^2$	0.31	1	0.31	21.61	0.0023		
	$B^2$	0.031	1	0.031	2.13	0.1880		
	$C^2$	0.58	1	0.58	39.78	0.0004		
	Residual	0.10	7	0.015				
	Lack of Fit	0.015	3	0.004975	0.23	0.8721		not significant
	Pure Error	0.087	4	0.022				
	Cor Total	6.92	16					

For  $Y_2$ , the *p*-values of single factors *A*, *B*, and *C* were < 0.0001, 0.1941, and < 0.0001, respectively, indicating that factors *A* and *C* had a significant effect on  $Y_2$ , while factor *B* had a non-significance. The *p*-values of two-factor interaction *AB*, *AC*, and *BC* were 0.4344, 0.3169, and 0.0037, respectively, indicating that factor *BC* had a significant effect on  $Y_2$ , while factors *AB* and *AC* had a non-significance.

In addition, the reliability of the model was further tested by  $R^2$ ,  $R_a^2$ ,  $R_p^2$  and C.V. The results obtained are shown in Table 9.

**Table 9.** Reliability test.

Model	Standard Deviation	Mean	$R^2$	$R_a^2$	$R_p^2$	C.V./%
$Y_1$	3.52	56.89	0.9865	0.9691	0.8666	6.19
$Y_2$	0.12	2.99	0.9853	0.9664	0.9459	4.03

As can be seen from Table 9, the  $R^2$  of models  $Y_1$  and  $Y_2$  were 0.9865 and 0.9853,  $R_a^2$  were 0.9691 and 0.9664,  $R_p^2$  were 0.8666 and 0.459, and C.V. were 6.19% and 4.03%, respectively, which indicated that the predicted data of the models were highly correlated with the tested data and that the models were well fitted.

The studentized outer residual is an indicator used in statistics to assess the goodness of fit of the regression model. This can be used to determine the degree of abnormality of the data in the regression model, and plays an important role in the diagnosis of the regression model. As illustrated in Figure 5, the studentized outer residuals of the two models exhibited a linear relationship, indicating that the models were well-fitted.

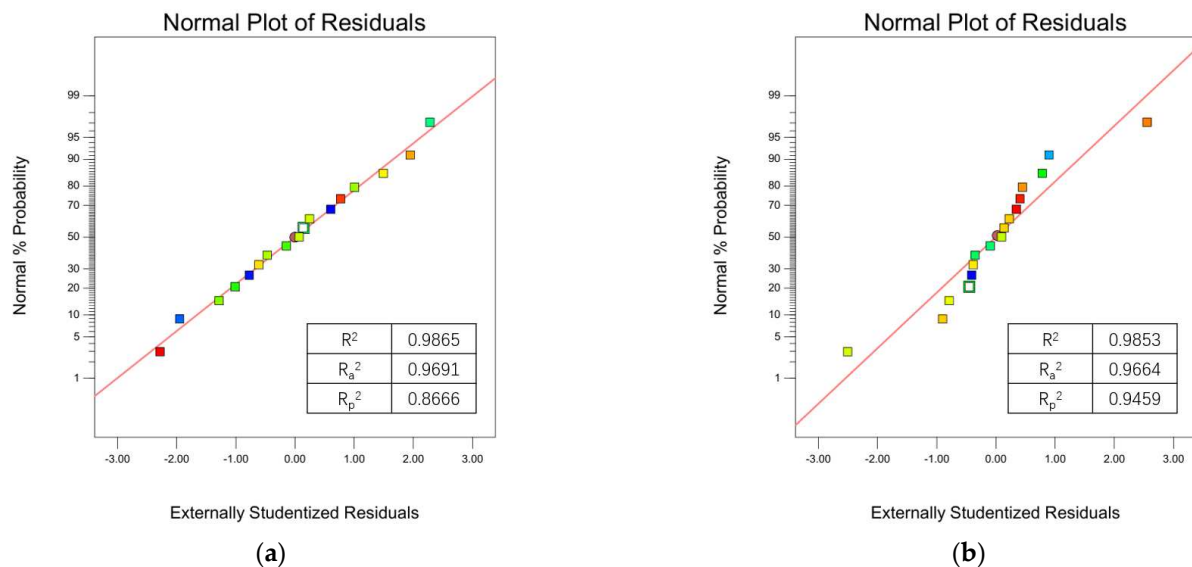


**Figure 5.** Normality of residuals. (a) Compressive strength; (b) Flexural strength.

### 3.3. Response Surface Analysis

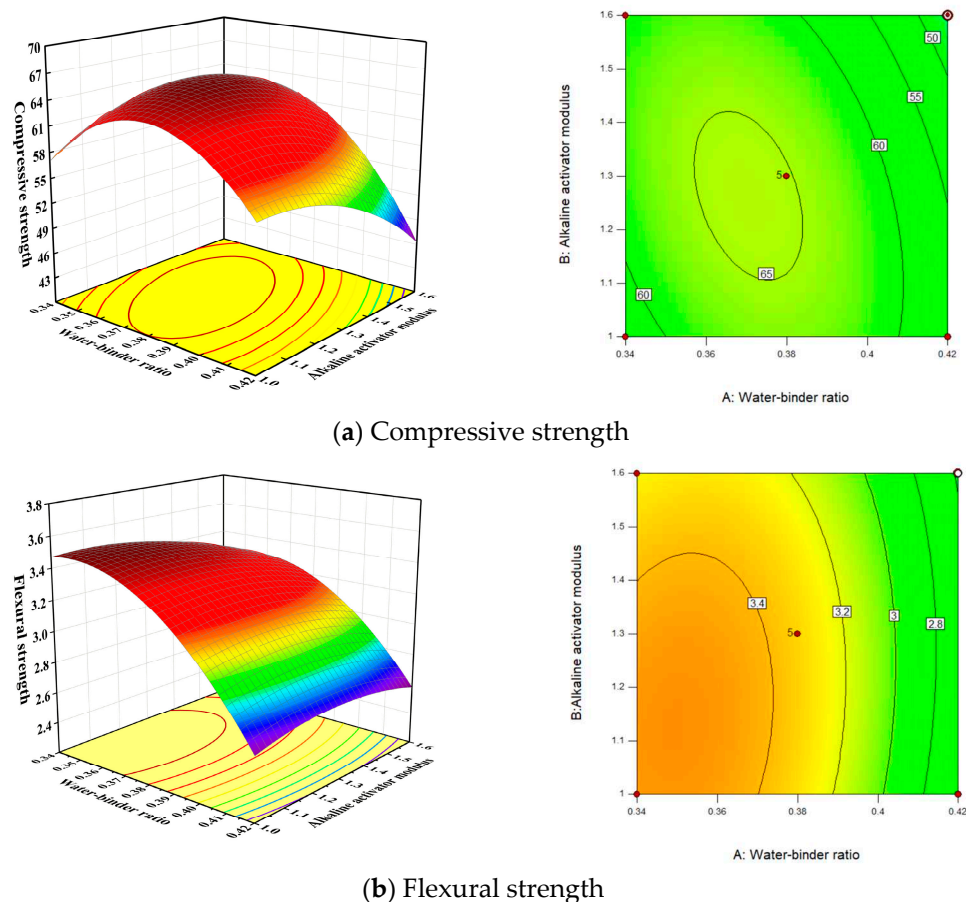
In order to ascertain the impact of each factor on the response values, 3D response surface plots of compressive strength and flexural strength of GPC were constructed (Figures 6–8).

Figure 6 illustrates the impact of the water–binder ratio and modulus of alkali exciter solution on the 28-day compressive strength and flexural strength of GPC when the slag mixing level is 0 (30%). It could be observed that, with an increase in the water–binder ratio, the compressive strength of GPC displayed a tendency from increase to decrease, while the flexural strength decreased continuously. As the modulus of the alkali exciter solution increased, the compressive strength and flexural strength displayed a pattern of initial growth followed by a decline. Comparatively, the effect of alkali exciter solution modulus on flexural strength was relatively minor.

Figure 7 illustrates the impact of water–binder ratio and slag replacement on the 28-day compressive strength and flexural strength of GPC when the modulus level of alkali excitant solution is 0 (1). As can be seen in Figure 7, with the increased water–binder ratio, the compressive strength of GPC initially raised before declining, while the flexural strength exhibited a consistent decline trend. Furthermore, the slag replacement has been demonstrated to significantly enhance the compressive and flexural strengths of GPC.

Figure 8 illustrates the impact of alkali exciter solution modulus and slag replacement on the 28-day compressive strength and flexural strength of GPC at a water–binder ratio of 0 (0.38). It could be observed from the figure that with the increase in slag replacement, the compressive strength and flexural strength of GPC were continuously enhanced. The effect of alkali exciter solution modulus on strength was contingent on the quantity of slag replacement. More specifically, when the quantity of slag replacement was less than 30%, the compressive strength and flexural strength of GPC would decrease with the increase in alkali exciter solution modulus; conversely, when the quantity of slag replacement was greater than 30%, the compressive strength and flexural strength of GPC would increase with the increase in alkali exciter solution modulus.

The water–binder ratio directly affects the workability and strength of GPC. When the water–binder ratio is excessive, a surplus of water remains in the specimen, which results in an increase in the internal porosity of the GPC. And the excess water hinders the reaction between the alkali activator and the silicon aluminum raw material, causing the sample to bleed and thus affecting the progress of the polymerization reaction. Furthermore, the excess water also increases the risk of drying and cracking and the excessive fluidity of the geopolymer slurry may lead to a decrease in the agglomeration and dispersion, which is also not conducive to the development of the strength of the GPC [59]. When the water–binder ratio is too low, insufficient water is presented during the reaction, which impairs the formation of the gel network. And the workability of GPC during mixing is poor, which makes the polymerization reaction unable to fully react in a short time [83]. The paste is consequently too viscous, making it difficult to flow and fill, which results in uneven distribution and the formation of bubbles. This would lead to the formation of pores and voids within the structure, reducing the strength of the GPC.



**Figure 6.** The effect of the interaction between water binder ratio and alkali activator modulus on strength.

Generally speaking, alkaline activators, which could stimulate the activity of silicate and aluminate, play an important role in the process of geological polymerization. The concentration, particle size and chemical properties of different activators would affect the formation rate and final structure of the polymers, which in turn affect the mechanical properties, chemical properties and environmental effects of the materials. However, in this study, it is found that the impact of the alkaline activator solution modulus was not as significant as the other two influencing factors. This was caused by the value range set in the test, especially within the modulus range of 1.0–1.6, all the resulted strengths of GPC were relatively high. The modulus of the alkali exciter was adjusted by varying the

quantity of sodium hydroxide added, i.e., as the quantity of sodium hydroxide increases, the content of  $\text{OH}^-$  ions and  $\text{Na}^+$  ions in the solution grows, and the modulus of the alkali exciter decreases. When the modulus of the alkaline activator solution exceeds an optimal range, the dissolution rates of both fly ash and slag diminish. This leads to a reduction in the amount of gel produced through polymerization, slowing the formation of the polymer structure, and an increase in the number of unreacted fly ash and slag particles. Conversely, as the modulus of the alkaline activator solution is reduced, the degree of silica-aluminate depolymerization increases with the increase in  $\text{OH}^-$  ions, thereby increasing the strength of the GPC [84]. However, when the critical value is exceeded, the excess  $\text{OH}^-$  ions would cause the condensation reaction to occur prematurely, resulting in the premature precipitation of the geopolymer gel and the encapsulation of the unreacted particles. This would lead to a decrease in the strength of the GPC [85].

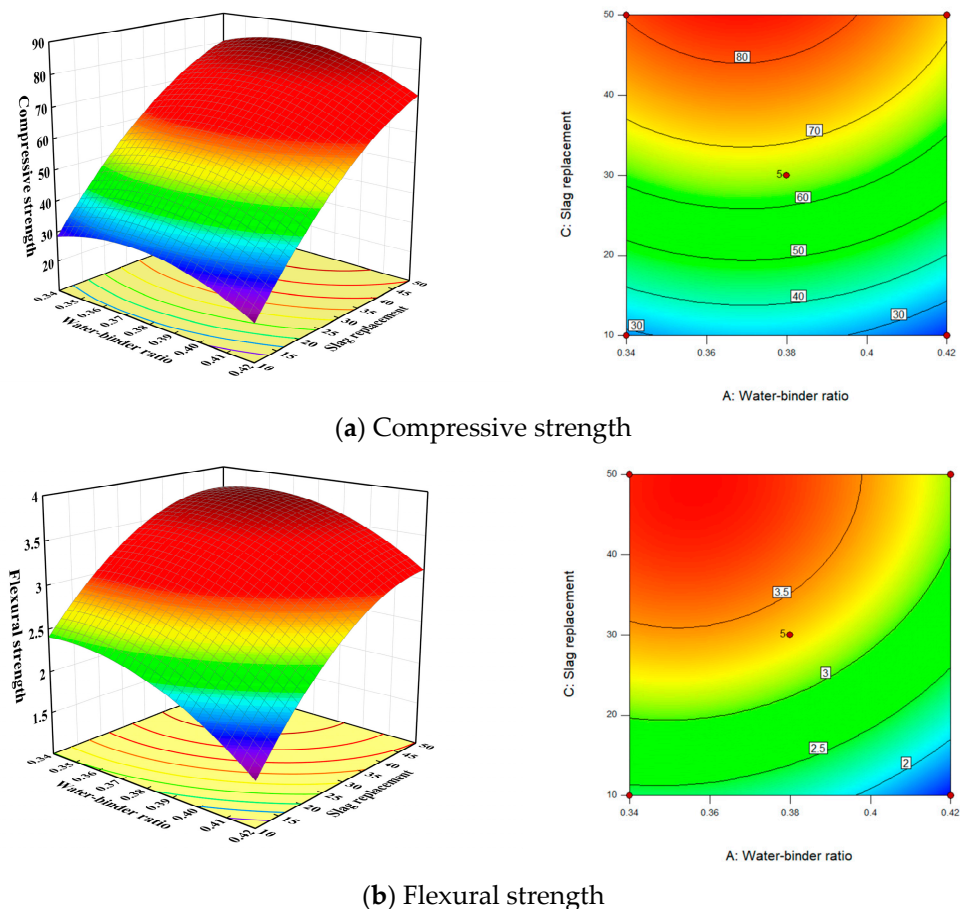


**Figure 7.** The influence of the interaction between water binder ratio and slag replacement on strength.

Slag has a higher density than fly ash, with stronger particle hardness and hydration strength than fly ash. Slag contains a great quantity of calcium elements, providing a substantial amount of  $\text{CaO}$  for the reaction.  $\text{CaO}$  is readily soluble, releasing a considerable quantity of  $\text{Ca}^+$  ions, which facilitates the formation of C-S-H and C-A-S-H gels. With the increase in slag proportion, the number of C-S-H gel increases, which increases the agglomeration degree of fly ash particles in the cementation reaction. Due to the bonding reaction, the aggregation degree of fly ash particles is higher and provides nucleation points for further reactions, thereby improving the strength of geopolymer concrete [86]. Therefore, the increase in slag replacement leads to a notable enhancement in strength [87–89].

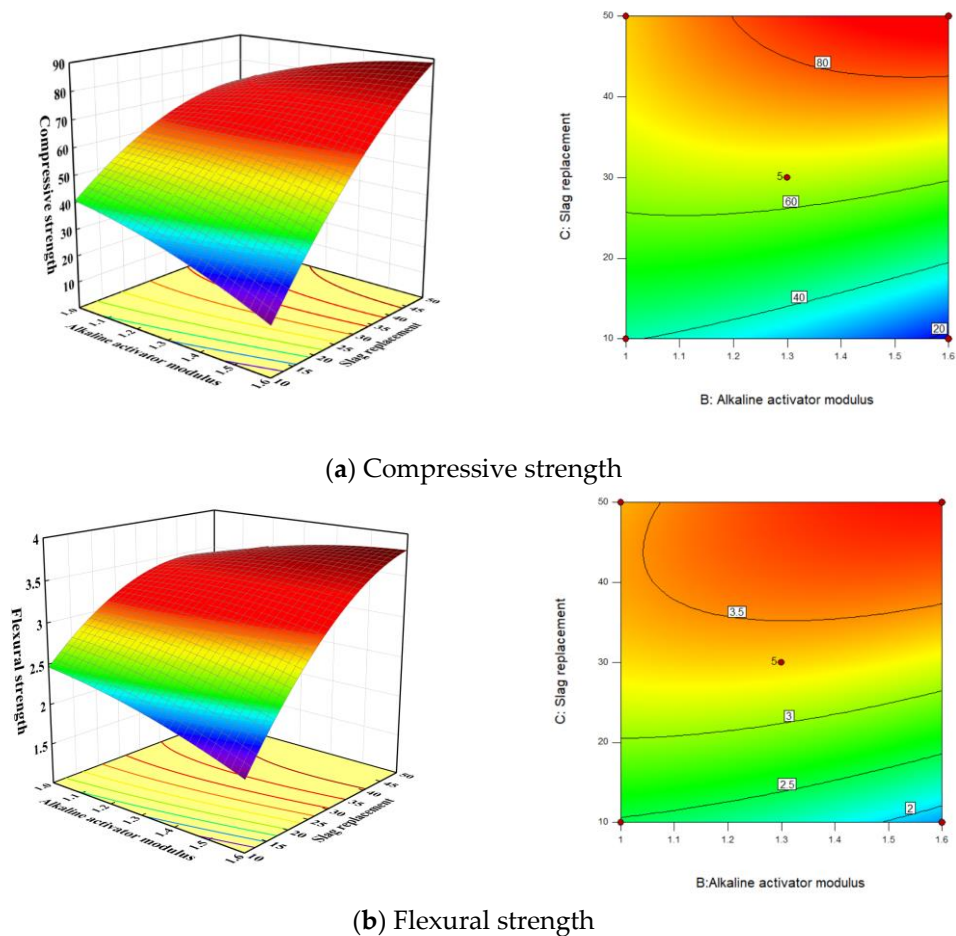


**Figure 8.** The effect of the interaction between alkali activator modulus and slag replacement on strength.

### 3.4. Multi-Objective Optimisation

Here, the joint expectation function was employed to identify the maximum response values and the corresponding combination of factor levels [66]. The multi-objective response problem is transformed into a single objective, whereby each independent variable is combined to form a composite function, which is subsequently optimized in order to achieve overall optimization [90].

The combined maximum value of compressive strength and flexural strength was taken as the desired objective. The factor level was within the original design level. The optimal mix ratio of GPC was sought through response surface optimization. According to the optimization results of the model, two groups of tests were conducted to verify the model's prediction and optimization ability. The optimal combinations and the compressive and flexural strengths obtained are presented in Table 10.

**Table 10.** Best mix ratio and its strength.

	Water–Binder Ratio	Alkaline Activator Modulus	Slag Replacement	Compressive Strength/MPa	Flexural Strength/MPa
Predicted value	3.5	1.54	47%	86.3	3.82
Tested value				82.5	4.02

From Table 10 we can see, that the correlation error between the predicted model's results and tested values were  $-4.4\%$  and  $5.2\%$ , respectively, for compressive and flex-

ural strengths, which proved that the prediction accuracy of the established response surface model.

### 3.5. Microstructure

The ANOVA of the response surface model in Section 3.2 indicated that the water–binder ratio and slag replacement had a significant effect on the compressive and flexural strengths of GPC.

In order to elucidate the mechanism of the effects of water–binder ratio (Figure 9), an SEM test was carried out for the specimens with an alkali-excitant modulus of 1.3, a slag replacement of 50%, and water–binder ratios of 0.34, 0.38, and 0.42.

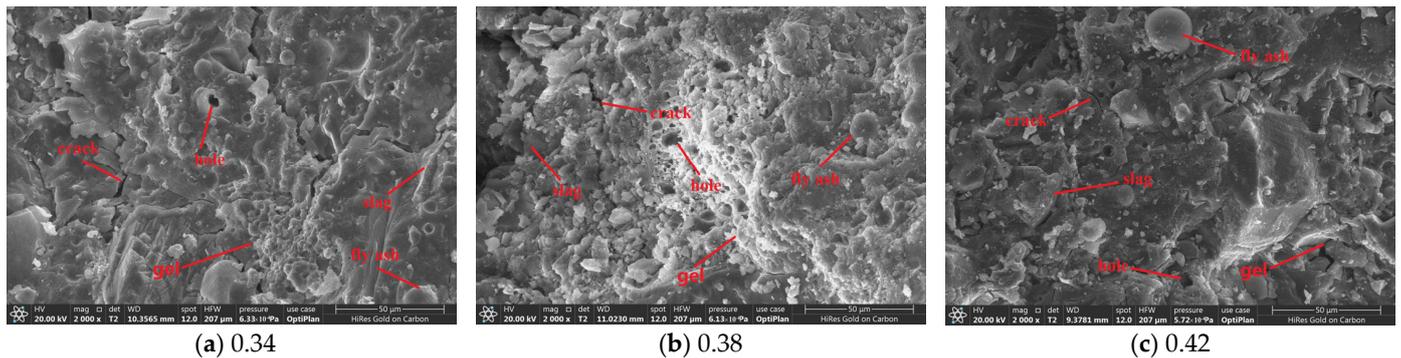


Figure 9. SEM images of GPC with different water–binder ratios.

Figure 9 illustrates that when the water–binder ratio was low (0.34), the consistency was markedly high, resulting in an uneven distribution and difficulty in discharging air bubbles. This would inevitably lead to the formation of holes and voids within the structure, which reduced the strength. When the water–binder ratio was too high (0.42), the paste was distributed more uniformly, but cracks were found in the structure, as well as small holes left by water evaporation, which also would lead to a reduction in the strength of GPC [91].

Similarly, an SEM test was also conducted for the specimens with a water–binder ratio of 0.38, an alkali exciter modulus of 1.3, and slag replacement of 10%, 30%, and 50% to study the mechanism of the effects of slag replacement (Figure 10).

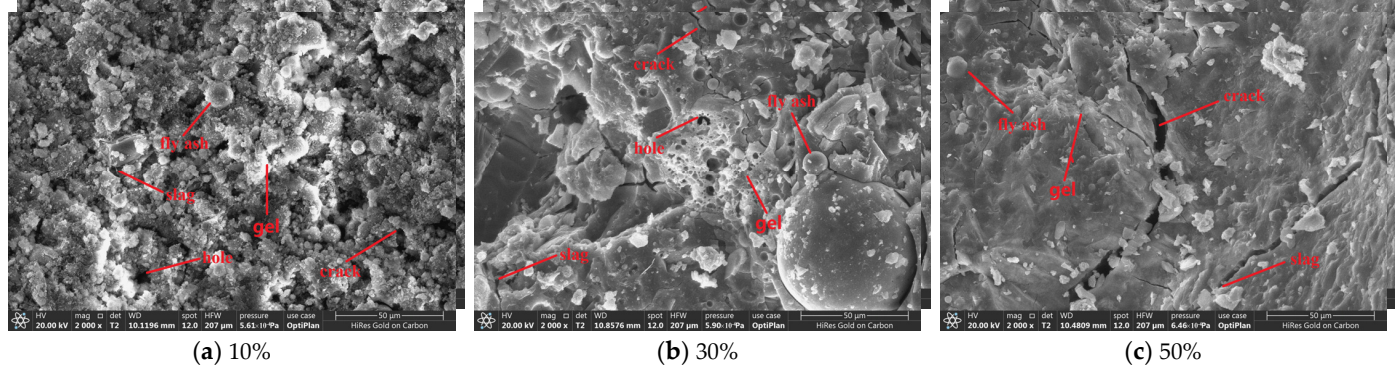


Figure 10. SEM images of GPC with different slag admixtures.

Figure 10 illustrates that when the slag replacement was low (10%), the microstructure of the GPC was highly porous, with numerous internal voids and numerous unreacted fly ash particles. Consequently, the reaction generated minimal C–S–H and C–A–S–H gel substances, and the strength of the GPC was significantly reduced. As the slag replacement ratio increased, the microstructure of GPC gradually became more compact, with a concomitant reduction in pore size [92]. However, when the slag replacement was excessive

(50%), it could be observed that the microstructure of GPC exhibited pronounced cracks. This may be attributed to the fact that with the increase in slag replacement, more heat was released, and the temperature difference caused cracks [93]. However, it also can be observed that the gel fills into the cracks, thereby suppressing the reduction in strength.

#### 4. Conclusions and Recommendations

- (1) Within the scope of the experimental design, the compressive strength would first increase and then decrease with the increase in the water–binder ratio, and would increase with the growth of slag replacement, while the flexural strength would increase with the decrease in the water–binder ratio and the increase in slag replacement. The impact of the alkaline activator solution modulus was not as significant as the other two influencing factors.
- (2) The strength of GPC would be influenced by the interaction among factors. When the slag replacement was high, the strength raised with the increase in the modulus of the alkaline exciter solution; conversely, when the slag replacement was low, the strength declined with the increase in the modulus of the alkaline exciter solution.
- (3) The water–binder ratio of 3.50, the modulus of alkaline exciter solution of 1.54, and the slag replacement of 47% were the optimal design of the proposed GPC.
- (4) Too high or too low water–binder ratio led to the appearance of pores and voids in the structure, which was detrimental to the formation of the gel network. The crumbly structure of GPC would be formatted when the slag replacement was too low, while cracks could occur in the structure when the slag replacement was too high.

Based on the research, the following recommendations were proposed:

- (1) An appropriate design method should be selected according to actual demand when optimizing the mix proportion of GPC.
- (2) The interaction between multiple influencing factors should be considered for the study of the performance of GPC.
- (3) In the future, nanotechnology might be used to improve the dispersibility and activity of fly ash and slag, thereby improving the microstructure, strength, and durability of geopolymer materials.

**Author Contributions:** Conceptualization, Z.Z. and C.W.; methodology, R.Z., C.W. and L.Z. (Lin Zhang); validation, R.Z., T.S. and K.M.; formal analysis, Z.Z. and L.Z. (Lu Zhang); data curation, Z.Z. and K.M.; investigation, Z.Z. and C.W.; writing—original draft preparation, Z.Z.; writing—review and editing, C.W. and C.V.A.; supervision, C.W. All authors have read and agreed to the published version of the manuscript.

**Funding:** This research was funded by Shandong Natural Science Foundation Project (ZR2020ME269, ZR2023ME169); and Key Research and Development Program of Shandong Province (2019GHY112076).

**Data Availability Statement:** The data used and/or analyzed during this study are available from the corresponding author on reasonable request.

**Conflicts of Interest:** The authors declare no conflict of interest.

#### References

1. Rambabu, D.; Sharma, S.K.; Akbar, M.A. Evaluation of roller compacted concrete for its application as high traffic resisting pavements with fatigue analysis. *Constr. Build. Mater.* **2023**, *401*, 132977. [[CrossRef](#)]
2. Makoond, N.; Setiawan, A.; Orton, S.L.; Adam, J.M. The effect of continuity reinforcement on the progression of collapse in reinforced concrete buildings. *Structures* **2024**, *61*, 105981. [[CrossRef](#)]
3. Filizadeh, R.; Hernandez, E.M.; Rosowsky, D.V. Risk-based framework for post-earthquake monitoring and evaluation of reinforced concrete bridges subject to multiple hazards. *Reliab. Eng. Syst. Saf.* **2024**, *245*, 109992. [[CrossRef](#)]
4. Almutairi, A.L.; Tayeh, B.A.; Adesina, A.; Isleem, H.F.; Zeyad, A.M. Potential applications of geopolymer concrete in construction: A review. *Case Stud. Constr. Mater.* **2021**, *15*, e00733. [[CrossRef](#)]
5. Ni, S.; Liu, H.; Li, Q.; Quan, H.Z.; Gheibi, M.; Fathollahi-Fard, A.M.; Tian, G. Assessment of the engineering properties, carbon dioxide emission and economic of biomass recycled aggregate concrete: A novel approach for building green concretes. *J. Clean. Prod.* **2022**, *365*, 132780. [[CrossRef](#)]

6. Biernacki, J.J.; Bullard, J.W.; Sant, G.; Banthia, N.; Brown, K.; Glasser, F.P.; Jones, S.; Ley, T.; Livingston, R.; Nicoleau, L.; et al. Cements in the 21st century: Challenges, perspectives, and opportunities. *J. Am. Ceram. Soc.* **2017**, *100*, 2746–2773. [[CrossRef](#)]
7. Yankelevsky, D.Z.; Karinski, Y.S.; Zhutovsky, S.; Feldgun, V.R. Isotropic triaxial tests of equal strength concrete with different mix compositions. *Constr. Build. Mater.* **2023**, *408*, 133717. [[CrossRef](#)]
8. Jin, H.; Cheng, L.; Liu, J.; Zhong, S. Investigation of natural diffusion behavior in concrete using iodide replacing chloride ions: The impact of mineral admixtures types and dosages. *J. Mater. Res. Technol.* **2024**, *29*, 1834–1861. [[CrossRef](#)]
9. Marey, H.; Kozma, G.; Szabó, G. Green concrete materials selection for achieving circular economy in residential buildings using system dynamics. *Clean. Mater.* **2024**, *11*, 100221. [[CrossRef](#)]
10. Khan, M.; Javed, M.F. Towards sustainable construction: Machine learning based predictive models for strength and durability characteristics of blended cement concrete. *Mater. Today Commun.* **2023**, *37*, 107428. [[CrossRef](#)]
11. Khankhaje, E.; Kim, T.; Jang, H.; Kim, C.S.; Kim, J.; Rafieizonooz, M. A review of utilization of industrial waste materials as cement replacement in pervious concrete: An alternative approach to sustainable pervious concrete production. *Heliyon* **2024**, *10*, e26188. [[CrossRef](#)] [[PubMed](#)]
12. Akbar, A.; Liew, K.M. Assessing recycling potential of carbon fiber reinforced plastic waste in production of eco-efficient cement-based materials. *J. Clean. Prod.* **2020**, *274*, 123001. [[CrossRef](#)]
13. Danish, A.; Torres, A.S.; Moro, C.; Salim, M.U. Hope or hype? Evaluating the environmental footprint of reclaimed fly ash in geopolymer production. *Resour. Conserv. Recycl.* **2024**, *205*, 107564. [[CrossRef](#)]
14. Li, C.; Cui, S.; Nie, Z.; Gong, X.; Wang, Z.; Itsubo, N. The LCA of portland cement production in China. *Int. J. Life Cycle Assess.* **2015**, *20*, 117–127. [[CrossRef](#)]
15. Azunna, S.U.; Aziz, F.N.; Al-Ghazali, N.A.; Rashid, R.S.M.; Bakar, N.A. Review on the mechanical properties of rubberized geopolymer concrete. *Clean. Mater.* **2024**, *11*, 100225. [[CrossRef](#)]
16. He, Z.; Shen, A.; Lyu, Z.; Li, Y.; Wu, H.; Wang, W. Effect of wollastonite microfibers as cement replacement on the properties of cementitious composites: A review. *Constr. Build. Mater.* **2020**, *261*, 119920. [[CrossRef](#)]
17. Jamora, J.B.; Go, A.W.; Gudia, S.E.L.; Giduquio, M.B.; Loretero, M.E. Evaluating the use of rice residue ash in cement-based industries in the Philippines—Greenhouse gas reduction, transportation, and cost assessment. *J. Clean. Prod.* **2023**, *398*, 136623. [[CrossRef](#)]
18. Olsson, J.A.; Miller, S.A.; Kneifel, J.D. A review of current practice for life cycle assessment of cement and concrete. *Resour. Conserv. Recycl.* **2024**, *206*, 107619. [[CrossRef](#)]
19. Sahoo, N.; Kumar, A. Design of solar cement plant for supplying thermal energy in cement production. *J. Clean. Prod.* **2023**, *426*, 139151. [[CrossRef](#)]
20. Andrew, R.M. Global CO<sub>2</sub> emissions from cement production, 1928–2018. *Earth Syst. Sci. Data* **2019**, *11*, 1675–1710. [[CrossRef](#)]
21. Zeyad, A.M. Sustainable concrete Production: Incorporating recycled wastewater as a green building material. *Constr. Build. Mater.* **2023**, *407*, 133522. [[CrossRef](#)]
22. Eti, S.; Dinçer, H.; Yüksel, S.; Uslu, Y.D.; Gökçalp, Y.; Kalkavan, H.; Mikhaylov, A.; Pinter, G. Determination of priority criteria in green building transformation: An analysis on the service industry. *Res. Glob.* **2023**, *7*, 100164. [[CrossRef](#)]
23. Hamada, H.M.; Al-Attar, A.A.A.; Yahaya, F.M.; Muthusamy, K.; Tayeh, B.A.; Humada, A.M. Effect of high-volume ultrafine palm oil fuel ash on the engineering and transport properties of concrete. *Case Stud. Constr. Mater.* **2020**, *12*, e00318. [[CrossRef](#)]
24. Davidovits, J. Properties of geopolymer cements. In Proceedings of the First International Conference on Alkaline Cements and Concretes, Scientific Research Institute on Binders and Materials, Kiev State Technical University, Kiev, Ukraine, 11–14 October 1994; pp. 131–149.
25. Alouani, M.E.L.; Saufi, H.; Aouan, B.; Bassam, R.; Alehyen, S.; Rachdi, Y.; Hadki, H.E.L.; Mabrouki, J.; Belaouad, S.; Ez-Zaki, H.; et al. A comprehensive review of synthesis, characterization, and applications of aluminosilicate materials-based geopolymers. *Environ. Adv.* **2024**, *16*, 100524. [[CrossRef](#)]
26. Kaze, R.C.; Naghizadeh, A.; Tchadjie, L.; Adesina, A.; Djobo, J.N.Y.; Nemaleu, J.G.D.; Kamseu, E.; Melo, U.C.; Tayeh, B.A. Lateritic soils based geopolymer materials: A review. *Constr. Build. Mater.* **2022**, *344*, 128157. [[CrossRef](#)]
27. Li, J.-S.; Zhang, W.; Lang, L.; Dong, C.-X.; Huang, K. Preparation and properties of geopolymer containing phosphoric acid-activated fly ash and mechanically-milled kaolinite: Experiments and density function theory. *J. Clean. Prod.* **2024**, *441*, 140992. [[CrossRef](#)]
28. Huang, D.; Liu, Z.; Lin, C.; Lu, Y.; Li, S. Effects and mechanisms of component ratio and cross-scale fibers on drying shrinkage of geopolymer mortar. *Constr. Build. Mater.* **2024**, *411*, 134299. [[CrossRef](#)]
29. Shamsol, A.L.S.; Apandi, N.M.; Zailani, W.W.A.; Izwan, K.N.K.; Zakaria, M.; Zulkarnain, N.N. Graphene oxide as carbon-based materials: A review of geopolymer with addition of graphene oxide towards sustainable construction materials. *Constr. Build. Mater.* **2024**, *411*, 134410. [[CrossRef](#)]
30. Izadifar, M.; Valencia, N.C.; Xiao, P.; Ukrainczyk, N.; Koenders, E. 3D Off-Lattice Coarse-Grained Monte Carlo Simulations for Nucleation of Alkaline Aluminosilicate Gels. *Materials* **2023**, *16*, 1863. [[CrossRef](#)]
31. Izadifar, M.; Ukrainczyk, N.; Koenders, E. Silicate Dissolution Mechanism from Metakaolinite Using Density Functional Theory. *Nanomaterials* **2023**, *13*, 1196. [[CrossRef](#)]
32. Afzali, S.A.E.; Shayanfar, M.A.; Ghanooni-Bagha, M.; Golafshani, E.; Ngo, T. The use of machine learning techniques to investigate the properties of metakaolin-based geopolymer concrete. *J. Clean. Prod.* **2024**, *446*, 141305. [[CrossRef](#)]

33. Hamed, Y.R.; Elshikh, M.M.Y.; Elshami, A.A.; Matthana, M.H.S.; Youssf, O. Mechanical properties of fly ash and silica fume based geopolymer concrete made with magnetized water activator. *Constr. Build. Mater.* **2024**, *411*, 134376. [[CrossRef](#)]
34. Anggraini, V.; Asadi, A.; Syamsir, A.; Huat, B.B.K. Three point bending flexural strength of cement treated tropical marine soil reinforced by lime treated natural fiber. *Measurement* **2017**, *111*, 158–166. [[CrossRef](#)]
35. Khair, S.; Rahman, S.M.A.; Shaikh, F.U.A.; Sarker, P.K. Evaluating lithium slag for geopolymer concrete: A review of its properties and sustainable construction applications. *Case Stud. Constr. Mater.* **2024**, *20*, e02822. [[CrossRef](#)]
36. Kumar, A.; Saravanan, T.J.; Bisht, K.; Kabeer, K.I.S.A. A review on the utilization of red mud for the production of geopolymer and alkali activated concrete. *Constr. Build. Mater.* **2021**, *302*, 124170. [[CrossRef](#)]
37. Alrowaili, Z.A.; Alnairi, M.M.; Olarinoye, I.O.; Alhamazani, A.; Alshammari, G.S.; Al-Buriahi, M.S. Radiation attenuation of fly ash and rice husk ash-based geopolymers as cement replacement in concrete for shielding applications. *Radiat. Phys. Chem.* **2024**, *217*, 111489. [[CrossRef](#)]
38. Feng, X.; Liu, N.; Lu, X. Investigation of un-calcined coal gangue together with ground granulated blast furnace slag and fly ash to ambient-curing production high-strength geopolymer. *J. Mater. Res. Technol.* **2023**, *25*, 3985–3997. [[CrossRef](#)]
39. Xu, W.; Niu, X.; Zhu, Y. Deformation behavior and damage evaluation of fly ash-slag based geopolymer concrete under cyclic tension. *J. Build. Eng.* **2024**, *86*, 108664. [[CrossRef](#)]
40. Deb, P.S.; Nath, P.; Sarker, P.K. Drying Shrinkage of Slag Blended Fly Ash Geopolymer Concrete Cured at Room Temperature. *Procedia Eng.* **2015**, *125*, 594–600. [[CrossRef](#)]
41. Xing, Z.Q. Study on Mechanical Properties and Durability Offiber-Polymer Mortar and Concrete. Doctoral Dissertation, Northeast Forestry University, Harbin, China, 2021.
42. Li, Z.; Zhang, Y. Development of Sustainable Cementitious Materials. In Proceedings of the International Workshop on Sustainable Development and Concrete Technology American Concrete Institute International, Northwestern University, Iowa State University, Changjiang Water Resources Commission, China Building Material Academy, Beijing, China, 20–21 May 2004.
43. Duxson, P.; Provis, J.L.; Lukey, G.C.; Deventer, J.S.J. The role of inorganic polymer technology in the development of ‘green concrete’. *Cem. Concr. Res.* **2007**, *37*, 1590–1597. [[CrossRef](#)]
44. Gopalakrishna, B.; Pasla, D. Development of metakaolin based high strength recycled aggregate geopolymer concrete. *Constr. Build. Mater.* **2023**, *391*, 131810. [[CrossRef](#)]
45. Niyazuddin, B.U. Mechanical and durability properties of standard and high strength geopolymer concrete using particle packing theory. *Constr. Build. Mater.* **2023**, *400*, 132722. [[CrossRef](#)]
46. Pratap, B.; Mondal, S.; Rao, B.H. NaOH molarity influence on mechanical and durability properties of geopolymer concrete made with fly ash and phosphogypsum. *Structures* **2023**, *56*, 105035. [[CrossRef](#)]
47. Upadhyay, D.; Chanda, A.; Thakkar, S. Mixture Design of High-Strength Geopolymer Concrete. *Mater. Today Proc.* **2023**, *93*, 335–339. [[CrossRef](#)]
48. Kanagaraj, B.; Anand, N.; Jerry, R.; Raj, R.S.; Andrushia, D.; Lubloy, E. Influence of protective coating on flexural behaviour of high strength self-compacting geopolymer concrete beams exposed to standard fire temperature. *Case Stud. Constr. Mater.* **2023**, *19*, e02468. [[CrossRef](#)]
49. Kanagaraj, B.; Anand, N.; Jerry, R.; Raj, R.S.; Lubloy, E. Axial compressive behaviour and physical characteristics of high strength self-compacting geopolymer concrete (HSGC) columns exposed to elevated temperature. *Constr. Build. Mater.* **2023**, *401*, 132866. [[CrossRef](#)]
50. Turkey, F.A.; Beddu, S.B.; Ahmed, A.N.; Al-Hubboubi, S.K. Effect of high temperatures on the properties of lightweight geopolymer concrete based fly ash and glass powder mixtures. *Case Stud. Constr. Mater.* **2022**, *17*, e01489. [[CrossRef](#)]
51. Javed, U.; Shaikh, F.U.A.; Sarker, P.K. Corrosive effect of HCl and H<sub>2</sub>SO<sub>4</sub> exposure on the strength and microstructure of lithium slag geopolymer mortars. *Constr. Build. Mater.* **2024**, *411*, 134588. [[CrossRef](#)]
52. Zhang, B. Durability of low-carbon geopolymer concrete: A critical review. *Sustain. Mater. Technol.* **2024**, *40*, e00882. [[CrossRef](#)]
53. Wasim, M.; Ngo, T.D.; Law, D. Durability performance of reinforced waste-based geopolymer foam concrete under exposure to various corrosive environments. *Case Stud. Constr. Mater.* **2021**, *15*, e00703.
54. Li, Q.; Wang, J.; Zhou, Z.; Du, P.; Zhang, X. Effect of BaCl<sub>2</sub> on the hydration properties of ultrahigh performance geopolymer concrete. *Constr. Build. Mater.* **2023**, *403*, 133074. [[CrossRef](#)]
55. Oyebisi, S.; Olutoge, F.; Kathirvel, P.; Oyaotuderekumor, I.; Lawanson, D.; Nwani, J.; Ede, A.; Kaze, R. Sustainability assessment of geopolymer concrete synthesized by slag and corncob ash. *Case Stud. Constr. Mater.* **2022**, *17*, e01665. [[CrossRef](#)]
56. Chen, G.; Zheng, D.-P.; Chen, Y.-W.; Lin, J.-X.; Lao, W.-J.; Guo, Y.-C.; Chen, Z.-B.; Lan, X.-W. Development of high performance geopolymer concrete with waste rubber and recycle steel fiber: A study on compressive behavior, carbon emissions and economical performance. *Constr. Build. Mater.* **2023**, *393*, 131988. [[CrossRef](#)]
57. Singh, S.; Sharma, S.K.; Akbar, M.A. Developing zero carbon emission pavements with geopolymer concrete: A comprehensive review. *Transp. Res. Part D Transp. Environ.* **2022**, *110*, 103436. [[CrossRef](#)]
58. Kumar, M.; Kumar, A.; Solanki, D.; Mungule, M. Low molarity geopolymer concrete: Effects on compressive strength, elastic modulus, sorptivity and chloride migration. *Constr. Build. Mater.* **2023**, *409*, 134065. [[CrossRef](#)]
59. Guo, T.; Zhang, G.; Ma, F.; Shen, P.; Wang, R.; Song, W.; Wang, L.; Han, P.; Bai, X. Mechanical properties and microstructure of red mud-coal metakaolin geopolymer concrete based on orthogonal tests. *J. Build. Eng.* **2023**, *79*, 107789. [[CrossRef](#)]

60. Chokkalingam, P.; El-Hassan, H.; El-Dieb, A.; El-Mir, A. Development and characterization of ceramic waste powder-slag blended geopolymer concrete designed using Taguchi method. *Constr. Build. Mater.* **2022**, *349*, 128744. [[CrossRef](#)]
61. Li, N.; Shi, C.; Zhang, Z.; Zhu, D.; Hwang, H.-J.; Zhu, Y.; Sun, T. A mixture proportioning method for the development of performance-based alkali-activated slag-based concrete. *Cem. Concr. Compos.* **2018**, *93*, 163–174. [[CrossRef](#)]
62. Abdullah, N.; Chin, N.L. Simplex-centroid mixture formulation for optimised composting of kitchen waste. *Bioresour. Technol.* **2010**, *101*, 8205–8210. [[CrossRef](#)]
63. GGencel, O.; del Coz Diaz, J.J.; Sutcu, M.; Koksall, F.; Rabanal, F.P.A.; Martinez-Barrera, G.; Brostow, W. Properties of gypsum composites containing vermiculite and polypropylene fibers: Numerical and experimental results. *Energy Build.* **2014**, *70*, 135–144. [[CrossRef](#)]
64. Nemati, M.; Nematzadeh, M.; Rahimi, S. Effect of fresh concrete compression technique on pre- and post-heating compressive behavior of steel fiber-reinforced concrete: Experiments and RSM-based optimization. *Constr. Build. Mater.* **2023**, *400*, 132786. [[CrossRef](#)]
65. Xie, L.; Zhou, Y.; Xiao, S.; Miao, X.; Murzataev, A.; Kong, D.; Wang, L. Research on basalt fiber reinforced phosphogypsum-based composites based on single factor test and RSM test. *Constr. Build. Mater.* **2022**, *316*, 126084. [[CrossRef](#)]
66. Ali, M.; Kumar, A.; Yvaz, A.; Salah, B. Central composite design application in the optimization of the effect of pumice stone on lightweight concrete properties using RSM. *Case Stud. Constr. Mater.* **2023**, *18*, e01958. [[CrossRef](#)]
67. Driouich, A.; Chajri, F.; Hassani, S.E.A.E.; Britel, O.; Belouafa, S.; Khabbazi, A.; Chaair, H. Optimization synthesis geopolymer based mixture metakaolin and fly ash activated by alkaline solution. *J. Non-Cryst. Solids* **2020**, *544*, 120197. [[CrossRef](#)]
68. Santana, H.A.; Neto, J.S.A.; Júnior, N.S.A.; Ribeiro, D.V.; Cilla, M.S.; Dias, C.M. Self-compacting geopolymer mixture: Dosing based on statistical mixture design and simultaneous optimization. *Constr. Build. Mater.* **2020**, *249*, 118677. [[CrossRef](#)]
69. Long, X.; Cai, L.; Li, W. RSM-based assessment of pavement concrete mechanical properties under joint action of corrosion, fatigue, and fiber content. *Constr. Build. Mater.* **2019**, *197*, 406–420. [[CrossRef](#)]
70. Rathnayaka, M.; Karunasinghe, D.; Gunasekara, C.; Wijesundara, K.; Lokuge, W.; Law, D.W. Machine learning approaches to predict compressive strength of fly ash-based geopolymer concrete: A comprehensive review. *Constr. Build. Mater.* **2024**, *419*, 135519. [[CrossRef](#)]
71. Ali, A.; Khan, Q.U.Z.; Mehboob, S.S.; Tayyab, A.; Hayyat, K.; Haq, I.U. Enhancing multi-objective mix design for GGBS-based geopolymer concrete with natural mineral blends under ambient curing: A Taguchi-Grey relational optimization. *Ain Shams Eng. J.* **2024**, *15*, 102708. [[CrossRef](#)]
72. Win, T.T.; Wattanapornprom, R.; Prasittisopin, L.; Pansuk, W.; Pheinsusom, P. Investigation of Fineness and Calcium-Oxide Content in Fly Ash from ASEAN Region on Properties and Durability of Cement–Fly Ash System. *Eng. J.* **2022**, *26*, 77–90. [[CrossRef](#)]
73. Gai, W.; Dai, F.; He, B.; Zhou, C.; Wei, M.; Liu, Y. Influence of GGBFS and alkali activators on macro-mechanical performance and micro-fracture mechanisms of geopolymer concrete in split Hopkinson pressure bar tests. *Constr. Build. Mater.* **2024**, *434*, 136736. [[CrossRef](#)]
74. Maaze, M.R.; Shrivastava, S. Design development of sustainable brick-waste geopolymer brick using full factorial design methodology. *Constr. Build. Mater.* **2023**, *370*, 130655. [[CrossRef](#)]
75. Driouich, A.; Hassani, S.E.A.E.; Labjar, H.; Kassbi, S.; Kambuyi, T.N.; Britel, O.; Sallek, B.; Digua, K.; Chroqui, R.; Chaair, H. Modeling and optimizing synthesis of irreversible gel by sol-gel using experimental design. *Phosphorus Sulfur Silicon Relat. Elem.* **2019**, *195*, 50–59. [[CrossRef](#)]
76. Balti, S.; Boudenne, A.; Hamdi, N. Characterization and optimization of eco-friendly gypsum materials using response surface methodology. *J. Build. Eng.* **2023**, *69*, 106219. [[CrossRef](#)]
77. Ojha, A.; Aggarwal, P. Durability performance of low calcium Flyash-Based geopolymer concrete. *Structures* **2023**, *54*, 956–963. [[CrossRef](#)]
78. Shi, X.; Zhang, C.; Wang, X.; Zhang, T.; Wang, Q. Response surface methodology for multi-objective optimization of fly ash-GGBS based geopolymer mortar. *Constr. Build. Mater.* **2022**, *315*, 125644. [[CrossRef](#)]
79. Jumaa, N.H.; Ali, I.M.; Nasr, M.S.; Falah, M.W. Strength and microstructural properties of binary and ternary blends in fly ash-based geopolymer concrete. *Case Stud. Constr. Mater.* **2022**, *17*, e01317. [[CrossRef](#)]
80. GB/T 50081-2019; Standard for Test Methods of Concrete Physical and Mechanical Properties. Research Institute of Standards and Norms Ministry of Housing and Urban-Rural Development: Beijing, China, 2019.
81. GB/T 50107-2010; Standard for Evaluation of Concrete Compressive Strength. Research Institute of Standards and Norms Ministry of Housing and Urban-Rural Development: Beijing, China, 2010.
82. He, H.; Cheng, S.; Chen, Y.; Lan, B. Compression performance analysis of multi-scale modified concrete based on response surface method. *Case Stud. Constr. Mater.* **2022**, *17*, e01312. [[CrossRef](#)]
83. Arioz, E.; Arioz, O.; Kockar, O.M. An Experimental Study on the Mechanical and Microstructural Properties of Geopolymers. *Procedia Eng.* **2012**, *42*, 100–105. [[CrossRef](#)]
84. Kanagaraj, B.; Anand, N.; Andrushia, A.D.; Lubloy, E. Investigation on engineering properties and micro-structure characteristics of low strength and high strength geopolymer composites subjected to standard temperature exposure. *Case Stud. Constr. Mater.* **2022**, *17*, e01608. [[CrossRef](#)]

85. Raza, M.H.; Khan, M.; Zhong, R.Y. Investigating the impact of alkaline activator on the sustainability potential of geopolymer and alternative hybrid materials. *Mater. Today Sustain.* **2024**, *26*, 100742. [[CrossRef](#)]
86. Lee, N.K.; Lee, H.K. Reactivity and reaction products of alkali-activated, fly ash/slag paste. *Constr. Build. Mater.* **2015**, *81*, 303–312. [[CrossRef](#)]
87. Waqas, R.M.; Butt, F.; Zhu, X.; Jiang, T.; Tufail, R.F. A Comprehensive Study on the Factors Affecting the Workability and Mechanical Properties of Ambient Cured Fly Ash and Slag Based Geopolymer Concrete. *Appl. Sci.* **2021**, *11*, 8722. [[CrossRef](#)]
88. Deb, P.S.; Nath, P.; Sarker, P.K. The effects of ground granulated blast-furnace slag blending with fly ash and activator content on the workability and strength properties of geopolymer concrete cured at ambient temperature. *Mater. Des.* **2014**, *62*, 32–39. [[CrossRef](#)]
89. Hussein, S.S.; Fawzi, N.M. Influence of using various percentages of slag on mechanical properties of fly ash-based geopolymer concrete. *J. Eng.* **2021**, *27*, 5067. [[CrossRef](#)]
90. Nadondu, B.; Surin, P.; Deeying, J. Multi-objective optimization on mechanical properties of glass-carbon and durian skin fiber reinforced poly(lactic acid) hybrid composites using the extreme mixture design response surface methodology. *Case Stud. Constr. Mater.* **2022**, *17*, e01675. [[CrossRef](#)]
91. Gorde, P.; Thongire, O.; Kadam, G.; Shekh, S.; Sonawane, V.; Kulkarni, D. Review of geopolymer concrete in high grade infrastructure construction. *Mater. Today Proc.* **2023**, *in press*. [[CrossRef](#)]
92. Kumar, S.; Kumar, R.; Mehrotra, S.P. Influence of granulated blast furnace slag on the reaction, structure and properties of fly ash based geopolymer. *J. Mater. Sci.* **2010**, *45*, 607–615. [[CrossRef](#)]
93. Fan, L.F.; Chen, D.K.; Zhong, W.L. Effects of slag and alkaline solution contents on bonding strength of geopolymer-concrete composites. *Constr. Build. Mater.* **2023**, *406*, 133391. [[CrossRef](#)]

**Disclaimer/Publisher’s Note:** The statements, opinions and data contained in all publications are solely those of the individual author(s) and contributor(s) and not of MDPI and/or the editor(s). MDPI and/or the editor(s) disclaim responsibility for any injury to people or property resulting from any ideas, methods, instructions or products referred to in the content.